

THE ENVIRONMENTAL DEPENDENCE OF STRUCTURES FOR MASSIVE GALAXIES FROM THE HYPER SUPRIME-CAM SURVEY

SONG HUANG (黃崧)¹, ALEXIE LEAUTHAUD¹, KEVIN BUNDY¹, MICHAEL STRAUSS², YEN-TING LIN³, RACHEL MANDELBAUM⁴

Draft version 0

ABSTRACT

TODO: Place holder; This is the abstract used for giving a talk.

Under the most popular formation scenario, the structures of massive central galaxies depend on environment at fixed stellar mass due to different assembly histories shaped by their host halos. Yet, clear evidence of such effect is still lacking. Using deep, multi-band images for a large sample of massive galaxies at $0.2 < z < 0.5$ from the Hyper Suprime-Cam (HSC) survey, we discover subtle, but systematic structural difference for massive galaxies in low and high mass haloes. The differences are consistent with richer merger history in more massive halos. We show that the average profiles of mass, shape, and color, along with relations among masses within different radius (as proxy of mass assembled at different time) can help us gain more insights of their assembly history, and the weak lensing analysis enabled by HSC survey further helps us connect the differences we find to the average halo properties.

Subject headings: galaxies: elliptical and lenticular, cD — galaxies: formation — galaxies: photometry — galaxies: structure — galaxies: surveys

1. INTRODUCTION

Scientific Background

- Massive galaxies are important cosmic probe and unique labs to study galaxy evolution.
- Briefly explain why massive early-type galaxies are important through the difficulties of stellar-halo mass relation and stellar mass function at the high-mass end.
- Brief summary of the current understanding of their cosmic assembly history.
- Explain why we should care about the environment, and why we expect to see some environmental dependence in the structure and other properties of massive galaxies.
- Brief review of the current observations. It is still not clear whether there is a clear environmental dependence.

Observational difficulties (a.k.a Why we need HSC)

- Explain why it is important to study the mass distribution of massive galaxies out to large physical radius; and, given their unique light profiles, why it is more difficult to study them compared to late-type galaxies.
- Very brief summary of past observational efforts, and why they are not good enough (Not enough number of really massive galaxy; Shallow images; Background subtraction issue; and stacking analysis can be dangerous as while)

Basic idea of this work

- Here we take advantages of the ambitious Hyper Suprime camera survey...

¹Kavli Institute for the Physics and Mathematics of the Universe, The University of Tokyo Institutes for Advanced Study, the University of Tokyo (Kavli IPMU, WPI), Kashwa 277-8583, Japan

²Princeton University Observatory, Peyton Hall, Princeton, NJ 08544, USA

³Institute of Astronomy and Astrophysics, Academia Sinica, P.O. Box 23-141, Taipei 10617, Taiwan

⁴Carnegie-Mellon University **TODO: correct affiliation here**

The paper is organized as follows. Section 2 gives a brief overview of the HSC observation and data reduction. We will also summarize the process of sample selection. In Section 3, we will describe the method for deriving the stellar mass surface density profile. The main results are summarized in Section 4. Section 5 provides discussions of the assumptions used in this work, the potentially interesting physical implications, and several future improvements, ending with a summary in Section 6.

All the magnitudes used here are in AB system (Oke & Gunn 1983), and are corrected for Galactic extinction using calibrations from Schlafly & Finkbeiner (2011). Within this work, we assume $H_0 = 70 \text{ km s}^{-1} \text{ Mpc}^{-1}$, $\Omega_m = 0.3$, and $\Omega_\Lambda = 0.7$.

2. OBSERVATIONS AND SAMPLE SELECTION

2.1. *The Hyper Suprime-Cam Survey*

The Subaru Strategic Program (SSP, REF) makes use of the new prime-focus camera, the Hyper Suprime-Cam (HSC; Miyazaki et al. 2012), on the 8.2-m Subaru telescope at Mauna Kea. Taking advantage of the large field of view (FoV; 1.5 deg in diameter) of HSC, this ambitious multi-layer photometric survey will cover $\sim 1400 \text{ deg}^2$ of sky in 5 broad bands ($g r i z Y$) to the depth of $r \sim 26$ mag in the WIDE part in the next few years. This work is based on the internal data release S15B, which covers ~ 100 square of degree of sky in all 5-band to the required depth of WIDE survey. The regions covered by this release are overlapped with several previous spectroscopic survey (e.g. SDSS/BOSS: Eisenstein et al. 2011, Alam et al. 2015; GAMA: Driver et al. 2011, Liske et al. 2015).

The data are processed with hscPipe 4.0.1, a derivative of the Large Synoptic Survey Telescope (LSST) pipeline (e.g. Ivezić et al. 2008; Axelrod et al. 2010), modified for use with

Suprime-Cam and Hyper Suprime-Cam. `hscPipe` first bias subtract, flat field, model background, and perform object detection and measurement on the single exposure data. Then, different exposures are warped onto a common World Coordinate System (WCS) and combined into final images with improved signal-to-noise ratio (SNR) after astrometric and photometric calibration. The pixel scale of the combined images is $0.168''$. The photometric calibration is based on data obtained from the Panoramic Survey Telescope and Rapid Response System (Pan-STARRS) 1 imaging survey (Schlafly et al. 2012, Tonry et al. 2012, Magnier et al. 2013). To achieve consistent deblending and photometry across all bands, the `hscPipe` will perform multi-band post-processing on the combined images. The footprints and peaks of detected sources on each band will be merged into a single catalog. This consistent set of peaks and footprints is used as starting point for deblend and measure objects on the combined images of each band. These measurements are then merged into a reference catalog. After fixing the centroids, shape, and other non-amplitude parameters of every object in this catalog, `hscPipe` will derive forced photometry measurements at each band. Details of `hscPipe` and the multi-band processing method will be presented in REF (Bosch et al. in prep.).

In Figure 1, we compare the false color (gri) images of three nearby massive ETGs from both SDSS and HSC surveys. The images are generated using similar scaling and color schemes, and clearly demonstrate HSC’s capability to reach to low surface brightness domain. In i -band (ignoring the slight difference in filter response curve), the HSC WIDE image is 2.5-3.0 magnitude deeper than SDSS on average. This gives us huge advantage in exploring the outskirt of massive ETGs given their extended, shallow outer surface brightness profiles.

Motivated by the requirement of weak lensing analysis, the i -band data typically has the best seeing in all five bands (the median seeing is around $\text{FWHM} \sim 0.8''$). Therefore, we will mostly use the i -band images to study the structure of galaxies.

2.2. Massive Central Galaxies in Different Environments

The main scientific goal of this work is to investigate mass assembly history of massive, central ETGs, and its dependence on environments (or host dark halo mass) through their the spatial distribution of stellar mass.

To achieve this goal, we will select $\log(M_*/M_\odot) > 11.5$ massive central galaxies within host halo mass larger and smaller than $\log(M_{\text{Halo}}/M_\odot) = 14.0$ at $0.3 < z < 0.5$. As both M_* - M_{Halo} relation and stellar mass function are still quite uncertain at $\log(M_*/M_\odot) > 11.5$, it is of great interest to investigate the structure of galaxies in this region carefully. And, this stellar mass cut can greatly reduce the contamination of satellites (e.g. van Uitert et al. 2016). Meanwhile, under the adopted cosmology, $1.0''$ equals 4.4 and 6.1 kpc at redshift 0.3 and 0.5. Therefore, this redshift range enables us to reliable measure the total stellar mass within the inner 5 to 10 kpc (where the “in-situ” component should still dominates) of massive galaxies at the high redshift end assuming the typical seeing of HSC data. At the same time, the depth of the data still allows to study the very outskirt (~ 100 kpc) of these galaxies at $z \sim 0.5$. Also, such limits on mass and redshift ensure us a sizeable sample while let us safely ignore significant mass growth and structural evolution (no star formation, lower merger rate et al. e.g. Bellstedt et al. 2016, Inagaki et al. 2015; but also see Bai et al.

2014; more discussion about this in Section 5).

Based on recent constraints of M_* - M_{Halo} relation (e.g. Leauthaud et al. 2012, Behroozi et al. 2013, Kravtsov et al. 2014), above $\log(M_*/M_\odot) = 11.5$, there is a large scatter of halo mass at fixed stellar mass. At $\log(M_{\text{Halo}}/M_\odot) < 14.0$, these massive galaxies are mostly the centrals of small groups; while at $\log(M_{\text{Halo}}/M_\odot) > 14.0$, they start to become the centrals of very massive groups and galaxy clusters. Limited by the sample size and the capability of measuring halo mass for individual central galaxy, we will simply separate the sample into two broad halo mass bins with the help of the `redMaPPer` cluster catalog⁵ (v5.10, e.g. Rykoff et al. 2014; Rozo et al. 2015). These clusters are selected from the SDSS DR8 photometric data using overdensity of red-sequence galaxies. For each cluster, the catalog provides robust estimations of photometric redshift z_Λ and richness Λ , along with the best candidate of the central galaxy (the one with the highest central probability P_{CEN}). Information about the identified member candidates is also provided separately. Please see Rozo & Rykoff (2014), ?, ? for more details about the performance of the `redMaPPer` cluster catalog. Several works (e.g. Saro et al. 2015; Farahi et al. 2016; Simet et al. 2016) have tried to calibrate the $M_{200,c}$ – Λ relation using different methods. Despite the slightly different calibrations derived, it is safe to assume that most clusters identified by `redMaPPer` ($\Lambda > 20$) have $\log(M_{200,c}/M_\odot) \geq 14.0$. Considering the typical uncertainty of richness, and the fact that `redMaPPer` catalog starts to become incomplete toward low richness ($\Lambda < 40$) end at $z > 0.33$, we will focus on the $\Lambda > 30$ clusters in this work. Based on the calibrations from Farahi et al. (2016) or Simet et al. (2016), such richness cut gives us haloes with $M_{200c} \geq 1.56 \pm 0.35 \times 10^{14} M_\odot$ or $M_{200c} \geq 1.60 \pm 0.11 \times 10^{14} M_\odot$. Therefore, `redMaPPer` can provide us a sample of massive central galaxies in $\log(M_{\text{Halo}}/M_\odot) \geq 14.0$ haloes. And, we assume that, in the same footprints and redshift range, the $\log(M_*/M_\odot) \geq 11.5$ galaxies outside `redMaPPer` clusters are most likely to be the central of $\log(M_{\text{Halo}}/M_\odot) < 14.0$ haloes.

According to Leauthaud et al. (2016), all $0.3 < z < 0.5$ and $\log(M_*/M_\odot) \geq 11.5$ galaxies should have $i_{\text{SDSS,cModel}} \leq 21.0$ mag. Ignoring the tiny difference in response curves between SDSS and HSC i -band filters, we started by selecting all galaxies with $i_{\text{HSC,cModel}} \leq 21.5$ in the regions that are covered in all five filters, and have already reached the expected depth of WIDE survey. The details of the HSC cModel photometry, and its performance will be described in REF Bosch et al. in. prep. It is quite similar to the SDSS cModel in principle as it also fits the total flux of an object using a combination of de Vaucouleur and exponential components after the PSF convolution is considered. For this work, we select objects that are classified as extended, have well defined centroids, do not fail during the deblending process, and have cModel magnitudes in all five bands. [Song: Should we discuss the impact of failed cModel photometry?] A series of quality control cuts are applied to remove objects that are affected by saturation, cosmic ray, other optical artifacts; and the ones that are too close to the edge of the field in all five bands (each criterion affects less than 8% of the entire sample). After these cuts, a total number of 1760845 galaxies left in the sample. This sample will be referred as `hscPho`.

We match this sample with the central galaxies of `redMaPPer` catalogs using a $1.0''$ radius, and it results in 704

⁵See: <http://risa.stanford.edu/redmapper/>

galaxies. A small fraction of redMaPPer centrals in the our footprints do not have matched object in our sample due to severe contamination from optical artifacts or bleeding trails from saturated objects. And slight change of the matching radius has no impact of this sample. For galaxy in this sample, the photometric redshift of the cluster is available for each of them; and for 72% of them, the spectroscopic redshift from SDSS DR8 is also provided by redMaPPer catalog when available. This sample of will be referred as redBCG in the rest of the paper.

For the vast majority of galaxies that are not the centrals of very massive haloes, we need other sources for their redshift estimations. Although there has been many efforts for deriving photometric redshift (photo- z) using HSC five-band photometry, it is still a working progress now, and its performance at $z \leq 0.5$ is expected to be less satisfying due to the lack of information at the shorter wavelength side of the 4000 break. Therefore, we will only rely on external spectroscopic redshifts (spec- z) for this work. The HSC database compiles a catalog of external spec- z for this data release by matching the detected objects with public data of several spectroscopic surveys (e.g. SDSS/BOSS; GAMA). Duplicated matches from different sources are merged through internal matching using 0.5'' radius. For each object, the quality information of the spec- z from different catalogs are homogenized into a single flag that indicates whether the redshift is secure, and only secure spec- z are used in this work.

We match the hscPho sample with this external spec- z catalog using a 1.0'' radius, and it leads to 116813 matched objects. Among these matches, there are 42696 objects at $0.3 \leq z \leq 0.5$. Most of these redshifts come from either SDSS or GAMA survey. To further exclude contamination from satellite galaxies, we aggressively remove all galaxies that could be associated with the redMaPPer clusters from this catalog. First, the catalog of redBCG central galaxies is merged with the catalog of their member galaxies. Then, through cross matching using 1.0'' radius, all hscPho galaxies that are within 2.5 Mpc of projected distance to any of cluster member are removed from the catalog. After this step, 29973 galaxies are left in the sample. We will refer this sample as nonBCG later.

The redBCG sample is also matched with external spec- z catalog in the same way, and we update the redshift of the central galaxies with external spec- z when it is available. For the unmatched ones, 3 of them have spec- z of BCG provided by the redMaPPer catalog (most likely due to different criteria during the selection of spec- z sample). For the rest, we use the photo- z of the cluster from the redMaPPer catalog instead. At $0.3 \leq z \leq 0.5$, there are 375 central galaxies left in the redBCG sample. Among them, 67 (17.9%) do not have spec- z . Using the central galaxies that have both spec- and photo- z , we estimate the median absolute redshift difference $|z_{\text{Photo}} - z_{\text{Spec}}|$ is ~ 0.01 (only 12 have absolute difference larger than 0.05; and the largest difference is ~ 0.12). Therefore, we expect the mixture of redMaPPer photo- z and spec- z results in no bias for the redBCG sample given the goal of this work.

At the same time, the spec- z for both redBCG and nonBCG samples both come from a heterogeneous catalog, which mainly consists of spec- z from SDSS/BOSS and GAMA survey. All the current HSC WIDE footprints overlap with the SDSS/BOSS survey, which is the most important spec- z

sources for this work. As the main scientific goal of BOSS survey is to use the spatial distribution of Luminous Red Galaxies (LRG) to map the large scale structure, it selects a large sample of massive ETGs in our redshift range. However, due to the complex selection criteria for different subsamples (e.g. the LOWZ and CMASS), its M_* completeness is not easy to estimate. Recently, through comparing with the Stripe 82 Massive Galaxy Catalog (S82-MGC; Bundy et al. 2015), Leauthaud et al. (2016) suggests that the BOSS spec- z is about 80% complete at $\log(M_*/M_\odot) \geq 11.6$ at $0.3 < z < 0.5$. The current WIDE data also greatly overlap with the GAMA survey in the G09, G12, and G15 fields. Thanks to the optimized spatial completeness and deeper limit magnitude in r -band (~ 19.8 mag) of the GAMA survey, it provides 14% of additional spec- z for our samples. However, due to the selection on fixed magnitude, its M_* completeness strongly depends on redshift and optical color. According to Taylor et al. (2011) (e.g. their Figure 6), the 80% completeness increases from $10^{10.8} M_\odot$ at $z \sim 0.3$ to $10^{12.0} M_\odot$ at $z \sim 0.5$. Although there must be systematic differences between the above two works, we can expect a reasonable overall M_* completeness ($\sim 80\%$) for our samples at $\log(M_*/M_\odot) \geq 11.6$. Later, we will further investigate the M_* completeness and the impact of deeper photometry on total stellar mass estimate. Considering the subtle differences in sources of redshift and M_* completeness between the redBCG and nonBCG samples, we will carefully match them in the M_* - z space before any comparison is conducted.

2.3. Stellar Masses from SED Fitting

To further select galaxies that are truly very massive central galaxies, we use the broadband Spectral Energy Distributions (SEDs) fitting (see Walcher et al. 2011 for a recent review) code iSEDFit⁶ (?) to provide estimations of average stellar mass-to-light ratio (M_*/L_*) and k -corrected photometry of our sample. iSEDFit takes a simplified Bayesian approach. In general, it first generates a large grid of SEDs from synthetic stellar population models by drawing randomly from the prior distributions of relevant parameters (e.g. age, metallicity, dust extinction, and star formation history). Based on these models, it uses the observed photometry and redshift to compute the statistical likelihood, and generate the posterior probability distribution (PDF) functions of each parameter. To get the best estimate of certain parameter, iSEDFit “integrates” the full PDF over all the other “nuisance” parameters. Then, the median value of the resulting marginalized PDF is used as the best value, while the $1-\sigma$ uncertainty is derived from the cumulative PDF. Please refer to ? for technical details and performance of iSEDFit. In this work, we derive average M_*/L_* using the Flexible Stellar Population Synthesis⁷ (FSPS; v2.4; Conroy & Gunn 2010a, Conroy & Gunn 2010b) model based on the MILES⁸ (Sánchez-Blázquez et al. 2006, Falcón-Barroso et al. 2011) stellar library and Chabrier (2003) IMF between 0.1 to $100 M_\odot$. We use the delayed- τ model with stochastic star burst as the form of star formation history (SFH). We adopt flat distribution between 0.5 to 14.0 Gyrs as prior for the look-back time when the star formation turned on. The exponential delayed time-scale (τ) is allowed to change between 0.1 to 3.0 with equal probability. The chance of random star burst is set at 0.2 for every 2 Gyrs. The duration of the star burst is draw

⁶<http://www.sos.siena.edu/jmoustakas/isedfit/>

⁷<http://scholar.harvard.edu/cconroy/sps-models>

⁸<http://www.iac.es/proyecto/miles/pages/stellar-libraries/miles-library.php>

from a logarithmic distribution between 0.03 to 0.3 Gyr; and the mass fraction formed in the burst is from a logarithmic distribution between 0.01 and 1.0. Such form of SFH is generally considered to be appropriate for massive quiescent galaxies at low redshift (e.g. Kauffmann et al. 2003). For stellar metallicity, we assume flat distribution between 0.004 to 0.03 (which is the highest metallicity allowed by FSPS models). And, the Calzetti et al. (2000) extinction law is adopted with a order two Gamma distribution of A_V between 0 to 2 magnitude. To achieve reasonably good sampling across these parameters, we generate 250000 models using `iSEDFit`.

In principle, these choices of priors could leave systematic effects in the estimate of stellar mass (e.g. Bernardi et al. 2016a). For low- z massive ETGs like the ones in our sample, the details form of SFH, importance of random star burst, and the dust extinction should not be major concern. However, the choices of stellar population models and IMF can still change the results systematically. More discussions on this can be found in Appendix A. In short:

1. Both FSPS+MILES and BC03 (Bruzual & Charlot 2003) models still have difficulties recovering the optical color involving filters at the red end (e.g $i-Y$), which could relate to the challenge for modern stellar population models to reproduce the optical color-color relation of red-sequence galaxies (e.g. Ricciardelli et al. 2012), or the shallower photometry of HSC-Y band data.
2. The BC03 provides slightly better overall χ^2 and systematically smaller M_* than the FSPS+MILES models. However, it is possible that the BC03 model tends to underestimate the M_*/L_* for a fraction of them as the estimate stellar age is unrealistically young for red, massive galaxies. Therefore, we still use the FSPS+MILES model as the fiducial one. But, switching to the BC03 model will not change any key result in this work.
3. The usage of Salpeter (1955) IMF results in systematically higher M_* (on average +0.25 dex of $\log(M_*/M_\odot)$). Although there are multiple lines of evidence that favor Salpeter or even more “bottom-heavy” IMF in the most massive ETGs (e.g. Conroy & van Dokkum 2012; Cappellari et al. 2012), we still present the main results using Chabrier IMF to accommodate galaxies with lower M_* in the sample, and to be as consistent as possible with a few other works. Also, the choice of IMF does not impact our results qualitatively.

Besides the priors for stellar population properties, different treatments of the light profile and accuracy of sky background subtraction are also important for the estimate of M_* as they strongly impact the estimate of total luminosity (e.g. Bernardi et al. 2013 and D’Souza et al. 2015). At the depth of SDSS, the default cModel photometry is already shown to be not very accurate at high- M_* end (e.g. Meert et al. 2015; Bernardi et al. 2016b) as it does not capture the extended envelope of these galaxies. As for HSC, it is much more challenging for cModel to recover the total luminosity of massive ETGs since the stellar envelope becomes even more extended for neither de Vaucouleur or exponential model to reproduce. However, the HSC cModel under the force-photometry mode can measure **average** color of the galaxy with great accuracy (e.g. Huang et al. in prep.), and provide us a reliable SED to estimate the **average** M_*/L_* . Considering this, we separate the process of estimating the total M_* of massive ETGs in our sample into two steps:

1. Firstly, using the redshift and cModel magnitude in five bands, we derive an initial estimate of the M_* of the galaxy. More importantly, we derive the **average** M_*/L_* in i -band of the galaxy, and use the best-fit SED to provide k -correction to the photometry.
2. In the next section, we will derive better estimate of total M_* using the more accurate total luminosity in i -band from integration of carefully measured 1-D surface brightness profile, and the average M_*/L_* from the SED fitting.

We choose i -band because it typically has the best seeing and image quality among all five bands, and within our redshift range, the i -band data can still be seen as reasonable tracer of underlying stellar mass distributions in rest-frame (at least for massive ETGs). In practice, the accuracy of this approach depends on the reliability of the average M_*/L_* , and whether the M_*/L_* of the extended envelope missed by cModel is similar to the average M_*/L_* from the inner part. It is well known that massive ETGs have negative optical color gradient which indicates a gradient of M_*/L_* (e.g. La Barbera et al. 2012; D’Souza et al. 2015). Although the color gradient at the very outskirt are still not well quantified, it is believed to be smooth and shallow, which is favoured by our method. Also, since we focus on the comparison between the redBCG and nonBCG, our results should remain intact as long as there is no significant differences of color gradient between these two samples. We will discuss more later but the initial result suggests that this is indeed the case. In principle, this is similar to the method adopted by the GAMA survey (Taylor et al. 2011), where the average M_*/L_* comes from SED fitting of PSF-matched aperture photometry from multi-band photometry while the better total luminosity relies on multi-band Sérsic model fitting (Kelvin et al. 2012).

[Song: Not sure if we want to show this here, but just leave it here for now.] The basic results from `iSEDFit` are summarized in Figure 2, where we compare the relations between initial estimates of M_* and (both luminosity and star formation weighted) stellar age, metallicity, and dust extinction. As expected, most galaxies in our samples are $\log(M_{*,\text{ini}}/M_\odot) \geq 11.2$ massive galaxies that have old age, high metallicity ($1.5 \times Z_\odot$ is the highest metallicity allowed), and low dust extinction. Given that we only have photometry from five optical bands, degeneracies among age, metallicity, and dust extinction are naturally expected. We will not use them for any scientific reason in this work, but to show that they behave reasonably.

Currently, the cModel photometry heavily underestimates the flux errors of bright objects like the low- z massive galaxies in our samples since it only considers the statistical error of the data, not the systematic uncertainties within the model-fitting process. Therefore such flux errors are not useful here as they leads to strongly biased PDF for M_* . Photometric tests using simulated galaxies suggest that, even at the very bright end, the average accuracy of cModel photometry is not better than 1%. Based on that, we supply `iSEDFit` with simplified flux errors assuming $S/N = 100$ for riz bands, and $S/N = 80$ for gY bands (that typically have shallower images). Given such assumption, the typical uncertainty of $\log(M_*/M_\odot)$ for both samples is around 0.08 to 0.10 dex at the high- M_* end.

From the `iSEDFit` results, we also derive the k -corrected luminosity and colors. **[Song: Will modify the Fig3c to only**

show the g-r and g-z color, and remove the dashed vertical lines, replace them with single vertical line indicating $\log M = 11.6$; r-z and i-y are just to show the problem of SED fitting at the red end] In Figure 3, we show the M_* , ini-color relations for k -corrected $g-r$ and $g-z$ colors, and compare their distributions for redBCG and nonBCG samples at $\log(M_*, \text{ini}/M_\odot) \geq 11.5$. At high- M_* end, both samples follow the same, tight red-sequence without much contamination from the “blue cloud”. No apparent offset between the color distributions of the two samples at fixed M_* also suggests that, within the region traced by cModel, the average stellar population of massive central galaxy does not significantly depends on host halo mass (or environment), which is consistent with recent result (e.g. Park et al. 2007).

2.4. Comparison with S82-MGC

Given the heterogeneous sources of redshift for both samples, we further investigate the M_* completeness issue by comparing with galaxies in the common regions with the S82-MGC sample. The S82-MGC sample matches the deeper SDSS photometric data in the Stripe 82 region (Annis et al. 2014) with the near infrared data from the United Kingdom Infrared Telescope Infrared Deep Sky Survey (UKIDSS; Lawrence et al. 2007). With the help of deeper photometry and accurate photo-z, the S82-MGC sample is complete to $\log(M_*/M_\odot) \geq 11.2$ at $z < 0.7$, making it perfect sample to verify the completeness of our samples.

We first match our hscPho sample with S82-MGC, and get 42090 common galaxies. Adopting the ZBEST in S82-MGC catalog, there are 20453 of them at $0.3 < z < 0.5$ (referred as s82Pho sample). To eliminate any possible systematic, we fit their HSC cModel SED in exactly the same way with our redBCG and nonBCG samples to get their M_* . The M_* from five-band HSC SED shows very good correlation with the S82-MGC SED (five optical bands from SDSS and NIR data from UKIDSS) fitting M_* (S82-MGC also used iSEDFit, with slightly different priors).

Then, we compute the volume number densities of galaxies with different stellar masses for redBCG, nonBCG, and s82Pho samples using a naive estimate of the current survey area (99 deg^2 for full-color, full-depth areas; we do not care about the absolute number density here, but only the relative trends with stellar mass). We also estimate the uncertainties of these distributions by bootstrap resampling the PDF of $\log(M_*/M_\odot)$ 10000 times.

We show the comparison in Figure 4. Given the completeness of the S82-MGC, we treat the distribution of s82Pho sample (green) at high- M_* end as the “intrinsic SMF”. The distribution of nonBCG sample starts to deviates from the s82Pho one below $\log(M_*/M_\odot) < 11.6$, suggesting small level of incompleteness. For the redBCG sample, its “SMF” behaves quite differently with the s82Pho one albeit its M_* completeness should be better thanks to the photo-z from redMaPPerCatalog. Since these massive central galaxies are rare objects at low- z , and are likely hosted by very massive haloes with a narrow $\log(M_{\text{Halo}}/M_\odot)$ distribution, such different behaviour could be intrinsic. We notice that the density distribution of redBCG sample also turns over around $\log(M_*/M_\odot) \sim 11.5$. It is safe to conclude that, above this mass threshold (before any total luminosity correction), our redBCG and nonBCG samples both have reasonably high completeness. Even so, we still match their $\log(M_*/M_\odot)$ distributions care-

fully to performance fair comparison.

3. DATA REDUCTION

3.1. 1-D Surface Brightness Profile

As mentioned in the introduction section, although 2-D model fitting

Basic ideas

- Briefly explain that 1-D surface brightness profile is a very old fashion, but robust and straightforward way to describe the light or mass distribution of a galaxy. Although it is not exactly “model-independent”, it indeed has the advantages of not easily affected by complex substructures within the galaxy comparing with the more popular 2-D modeling method.
- Due to the uniquely extended nature of the light distributions of these massive ETGs, it is still unclear which is the most appropriate 2-D model for them (Can not be well described by 1-Sérsic model).

Step by step description

- Generation of cutout image in multiple bands:

1. Choice of image size: make sure that the cutout covers out to at least 500 kpc from the center of the galaxy.

2. Also generate the bad pixel masks, and the reconstructed PSF model for the galaxy center.

- Generation of object masks:

1. Briefly explain why we need to our own photometry instead of just using the cModel results from the HSC pipeline.

2. We need two kinds of masks: mask of all objects that will be used to measure the sky value; mask of objects expect for the central galaxy we want to derive surface brightness profile. Briefly describe their requirements.

3. Object detection using SEP Python library.

- Re-measurement and correction of sky background:

3.2. Stellar Mass Corrected for Total Luminosity

- Compare stellar mass from integration of 1-D profile and the cModel photometry
- Stellar mass, redshift, K-corrected color distributions.
- Red sequence properties
- Potential “contaminations” from disc galaxies

TODO: Justify why we can assume most very massive galaxies in $\Lambda < 20$ haloes are central galaxies

4. RESULTS

4.1. Impact of deep photometry on the luminosity and stellar mass function

4.2. Comparison of stellar mass density profiles

Brief summary of the process of sample matching

- 4.2.1. *Using stellar mass derived from the GAMA survey*
- 4.2.2. *Using stellar mass within 10 kpc aperture*
- 4.2.3. *Using stellar mass within 100 kpc aperture*
- 4.3. *Relations between stellar mass within different physical apertures*
- 4.4. *M_* – R_{50} relation*

5. DISCUSSION

5.1. Implications on Assembly History of Massive Galaxies

Comparison of mass profiles with previous studies at high redshift

- 5.2. *Ellipticity Profiles*
- 5.3. *The Impact of M/L Gradient*
- 5.4. *M_* and Structural Evolution between $0.3 < z < 0.5$*
- 5.5. *Impact from “Fossil Galaxies”*

“Fossil galaxy” is the most massive galaxy in a “fossil group/cluster” system. According to the commonly adopted definition, “fossil” systems are the group or cluster with high X-ray luminosity and large magnitude gap between the two brightest galaxies (REF: Ponman1994; Jones2003). Both observations and simulations suggest that they could represent the final stage of the hierarchical merging process in a group/cluster mass halo that is formed at very early epoch (e.g. REF: Khosroshahi2004, 2007; DOnghia2005; Dariush2007). Under this interpretation, at fixed halo mass, the central galaxy of a fossil system typically has larger stellar mass than the one in normal system (e.g. Harrison2012), as it has “consumed” most satellites early on; However, the “low richness” of a fossil system makes it difficult for red-sequence finder like `redMaPPer` to reliably identify (e.g. Figure 17 of Sadibekova2014). If some massive ETGs in our nonBCG sample are actual the centrals galaxies of fossil clusters, it could bias our conclusions about the relation between strcutre and “environment”.

Although it is possible that fossil systems formed earlier than normal clusters, the difference in detailed merging history is still unclear, hence it is hard to imagine the structural differences between fossil central galaxies and regular BCGs with same M_* . Naively speaking, more frequent mergers for fossil centrals should result in more extended stellar envelope. However, the distributions of epoch and mass-ratio of those mergers also matter.

The lack of any difference in stellar population properties may suggest It is still not clear how the mass assembly history of fossil central

5.6. Connection and Difference with the Intra-Cluster Light

5.7. Massive satellites of the $\Lambda > 20$ haloes

[Song: TBD:optional]

5.8. Future improvements

- 1. *Improvements of HSC data reduction: better sky modeling; `redMaPPer` clusters using HSC photometry.*
- 2. *Comparison with 2-D image modeling method.*
- 3. *“Correct” the PSF smearing effect at the center with the help of residual correct 2-D model.*

6. SUMMARY

The Hyper Suprime-Cam (HSC) collaboration includes the astronomical communities of Japan and Taiwan, and Princeton University. The HSC instrumentation and software were developed by the National Astronomical Observatory of Japan (NAOJ), the Kavli Institute for the Physics and Mathematics of the Universe (Kavli IPMU), the University of Tokyo, the High Energy Accelerator Research Organization (KEK), the Academia Sinica Institute for Astronomy and Astrophysics in Taiwan (ASIAA), and Princeton University. Funding was contributed by the FIRST program from Japanese Cabinet Office, the Ministry of Education, Culture, Sports, Science and Technology (MEXT), the Japan Society for the Promotion of Science (JSPS), Japan Science and Technology Agency (JST), the Toray Science Foundation, NAOJ, Kavli IPMU, KEK, ASIAA, and Princeton University.

Funding for SDSS-III has been provided by the Alfred P. Sloan Foundation, the Participating Institutions, the National Science Foundation, and the U.S. Department of Energy. The SDSS-III web site is <http://www.sdss3.org>. SDSS-III is managed by the Astrophysical Research Consortium for the Participating Institutions of the SDSS-III Collaboration including the University of Arizona, the Brazilian Participation Group, Brookhaven National Laboratory, University of Cambridge, University of Florida, the French Participation Group, the German Participation Group, the Instituto de Astrofisica de Canarias, the Michigan State/Notre Dame/JINA Participation Group, Johns Hopkins University, Lawrence Berkeley National Laboratory, Max Planck Institute for Astrophysics, New Mexico State University, New York University, Ohio State University, Pennsylvania State University, University of Portsmouth, Princeton University, the Spanish Participation Group, University of Tokyo, University of Utah, Vanderbilt University, University of Virginia, University of Washington, and Yale University.

TODO: Full acknowledgement

- Acknowledgements for Kevin and Alexie’s funding
- Acknowledgements for the Python libraries

This research made use of `Astropy`, a community-developed core Python package for Astronomy (Astropy Collaboration, 2013); `sep` Source Extraction and Photometry in Python (Barbary et al. 2015).

REFERENCES

- Alam, S., Albareti, F. D., Allende Prieto, C., et al. 2015, ApJS, 219, 12
 Annis, J., Soares-Santos, M., Strauss, M. A., et al. 2014, ApJ, 794, 120
 Axelrod, T., Kantor, J., Lupton, R. H., & Pierfederici, F. 2010, in Proc. SPIE, Vol. 7740, Software and Cyberinfrastructure for Astronomy, 774015
 Bai, L., Yee, H. K. C., Yan, R., et al. 2014, ApJ, 789, 134
 Barbary, Boone, & Deil. 2015, sep: v0.3.0

- Behroozi, P. S., Wechsler, R. H., & Conroy, C. 2013, ApJ, 770, 57
 Bellstedt, S., Lidman, C., Muzzin, A., et al. 2016, MNRAS, 460, 2862
 Bernardi, M., Meert, A., Sheth, R. K., et al. 2016a, ArXiv e-prints
 —. 2016b, MNRAS, 455, 4122
 —. 2013, MNRAS, 436, 697
 Bruzual, G., & Charlot, S. 2003, MNRAS, 344, 1000

- Bundy, K., Leauthaud, A., Saito, S., et al. 2015, ApJS, 221, 15
- Calzetti, D., Armus, L., Bohlin, R. C., et al. 2000, ApJ, 533, 682
- Cappellari, M., McDermid, R. M., Alatalo, K., et al. 2012, Nature, 484, 485
- Chabrier, G. 2003, PASP, 115, 763
- Conroy, C., & Gunn, J. E. 2010a, FSPS: Flexible Stellar Population Synthesis, Astrophysics Source Code Library
—. 2010b, ApJ, 712, 833
- Conroy, C., & van Dokkum, P. G. 2012, ApJ, 760, 71
- Driver, S. P., Hill, D. T., Kelvin, L. S., et al. 2011, MNRAS, 413, 971
- D'Souza, R., Vegetti, S., & Kauffmann, G. 2015, MNRAS, 454, 4027
- Eisenstein, D. J., Weinberg, D. H., Agol, E., et al. 2011, AJ, 142, 72
- Falcón-Barroso, J., Sánchez-Blázquez, P., Vazdekis, A., et al. 2011, A&A, 532, A95
- Farahi, A., Evrard, A. E., Rozo, E., Rykoff, E. S., & Wechsler, R. H. 2016, MNRAS, 460, 3900
- Inagaki, T., Lin, Y.-T., Huang, H.-J., Hsieh, B.-C., & Sugiyama, N. 2015, MNRAS, 446, 1107
- Ivezic, Z., Tyson, J. A., Abel, B., et al. 2008, ArXiv e-prints
- Kauffmann, G., Heckman, T. M., White, S. D. M., et al. 2003, MNRAS, 341, 54
- Kelvin, L. S., Driver, S. P., Robotham, A. S. G., et al. 2012, MNRAS, 421, 1007
- Kravtsov, A., Vikhlinin, A., & Meshcheryakov, A. 2014, ArXiv e-prints
- La Barbera, F., Ferreras, I., de Carvalho, R. R., et al. 2012, MNRAS, 426, 2300
- Lawrence, A., Warren, S. J., Almaini, O., et al. 2007, MNRAS, 379, 1599
- Leauthaud, A., Tinker, J., Bundy, K., et al. 2012, ApJ, 744, 159
- Leauthaud, A., Bundy, K., Saito, S., et al. 2016, MNRAS, 457, 4021
- Liske, J., Baldry, I. K., Driver, S. P., et al. 2015, MNRAS, 452, 2087
- Magnier, E. A., Schlaflay, E., Finkbeiner, D., et al. 2013, ApJS, 205, 20
- Meert, A., Vikram, V., & Bernardi, M. 2015, MNRAS, 446, 3943
- Miyazaki, S., Komiyama, Y., Nakaya, H., et al. 2012, in Proc. SPIE, Vol. 8446, Ground-based and Airborne Instrumentation for Astronomy IV, 84460Z
- Oke, J. B., & Gunn, J. E. 1983, ApJ, 266, 713
- Park, C., Choi, Y.-Y., Vogele, M. S., et al. 2007, ApJ, 658, 898
- Ricciardelli, E., Vazdekis, A., Cenarro, A. J., & Falcón-Barroso, J. 2012, MNRAS, 424, 172
- Rozo, E., & Rykoff, E. S. 2014, ApJ, 783, 80
- Rozo, E., Rykoff, E. S., Becker, M., Reddick, R. M., & Wechsler, R. H. 2015, MNRAS, 453, 38
- Rykoff, E. S., Rozo, E., Busha, M. T., et al. 2014, ApJ, 785, 104
- Salpeter, E. E. 1955, ApJ, 121, 161
- Sánchez-Blázquez, P., Peletier, R. F., Jiménez-Vicente, J., et al. 2006, MNRAS, 371, 703
- Saro, A., Bocquet, S., Rozo, E., et al. 2015, MNRAS, 454, 2305
- Schlaflay, E. F., & Finkbeiner, D. P. 2011, ApJ, 737, 103
- Schlaflay, E. F., & Finkbeiner, D. P. 2012, ApJ, 756, 158
- Simet, M., McClintock, T., Mandelbaum, R., et al. 2016, ArXiv e-prints
- Taylor, E. N., Hopkins, A. M., Baldry, I. K., et al. 2011, MNRAS, 418, 1587
- Tonry, J. L., Stubbs, C. W., Lykke, K. R., et al. 2012, ApJ, 750, 99
- van Uitert, E., Cacciato, M., Hoekstra, H., et al. 2016, MNRAS, 459, 3251
- Walcher, J., Groves, B., Budavári, T., & Dale, D. 2011, Ap&SS, 331, 1

APPENDIX

- A. DERIVE AVERAGE MASS-TO-LIGHT RATIO USING `ISEDFIT`
 B. EXTRACTION OF 1-D SURFACE BRIGHTNESS PROFILE

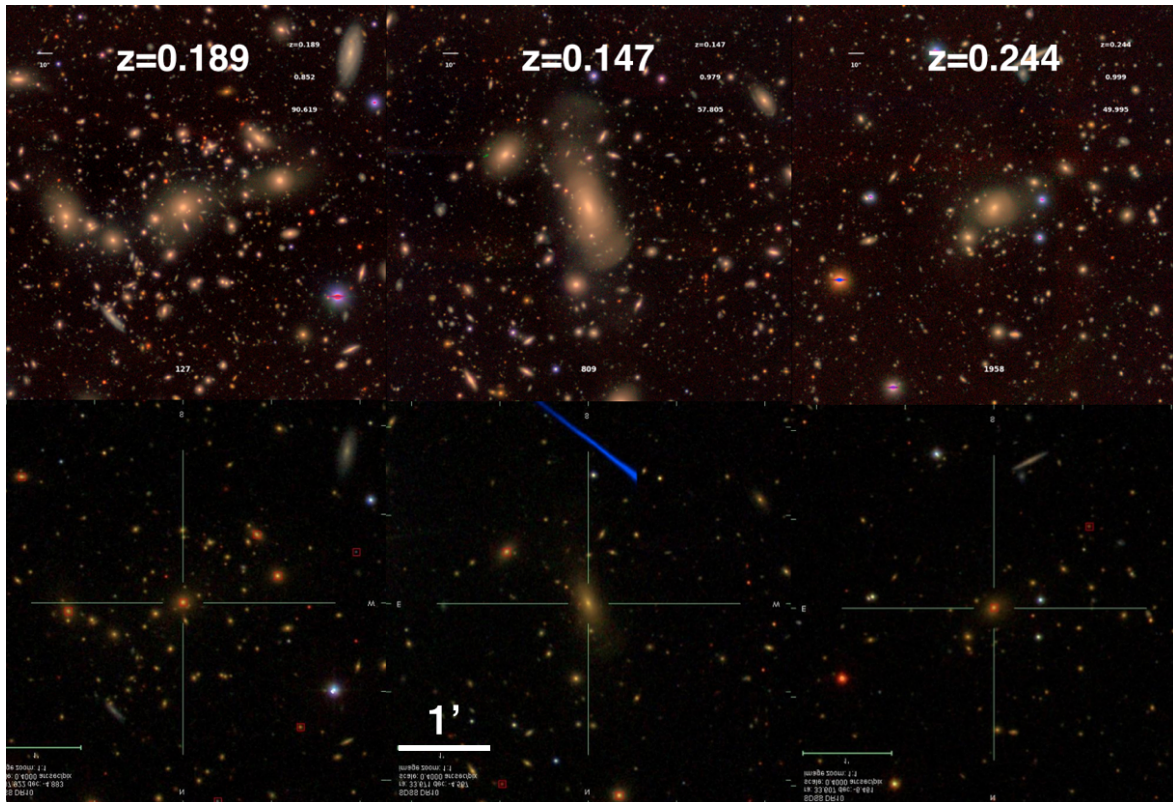
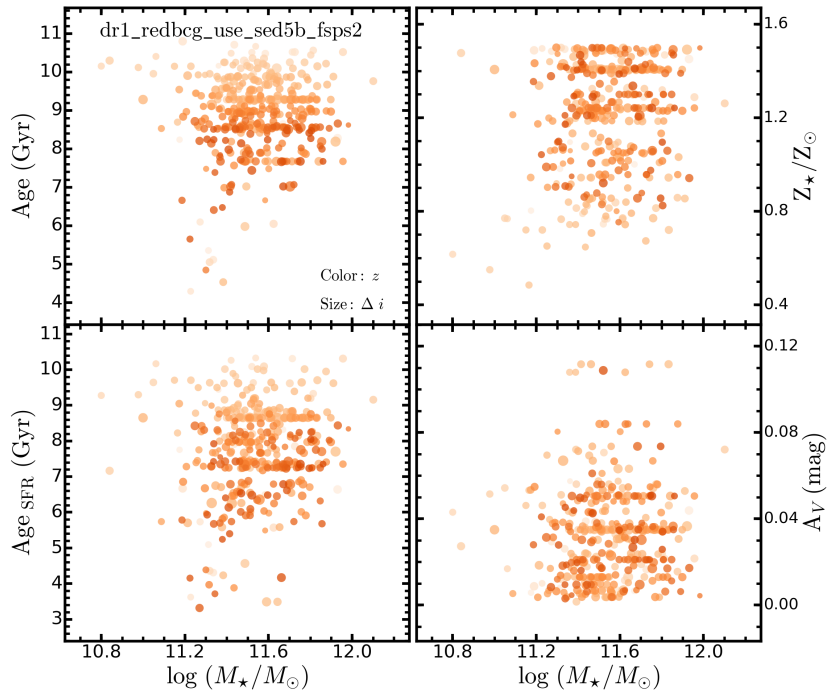
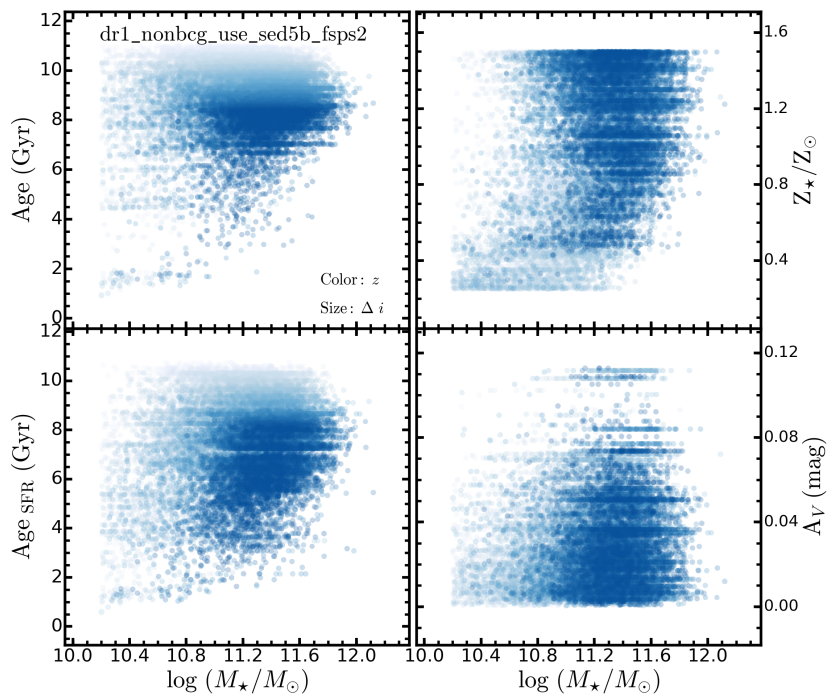


FIG. 1.— Figure.1TODO: Caption

FIG. 2A.— Figure.2a**TODO: Caption**FIG. 2B.— Figure.2b**TODO: Caption**

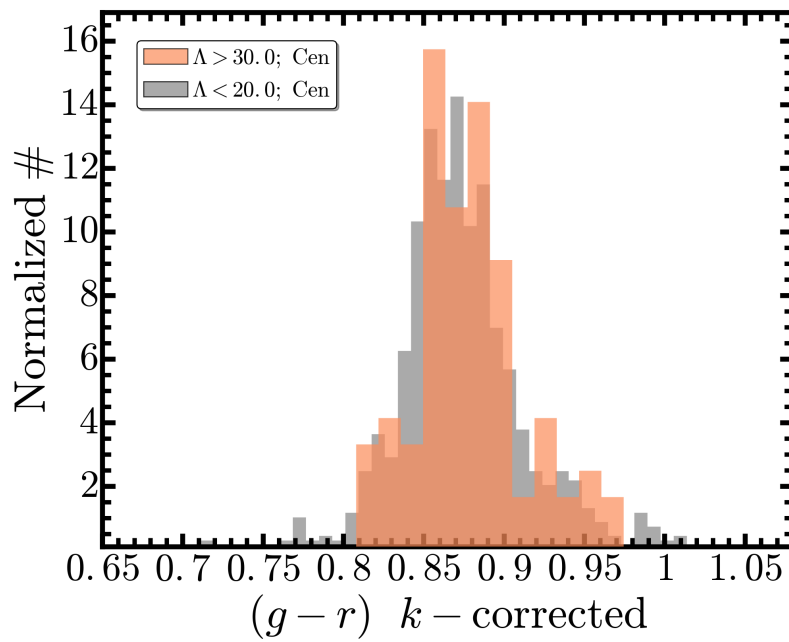


FIG. 3A.— Figure.3a TODO: Caption

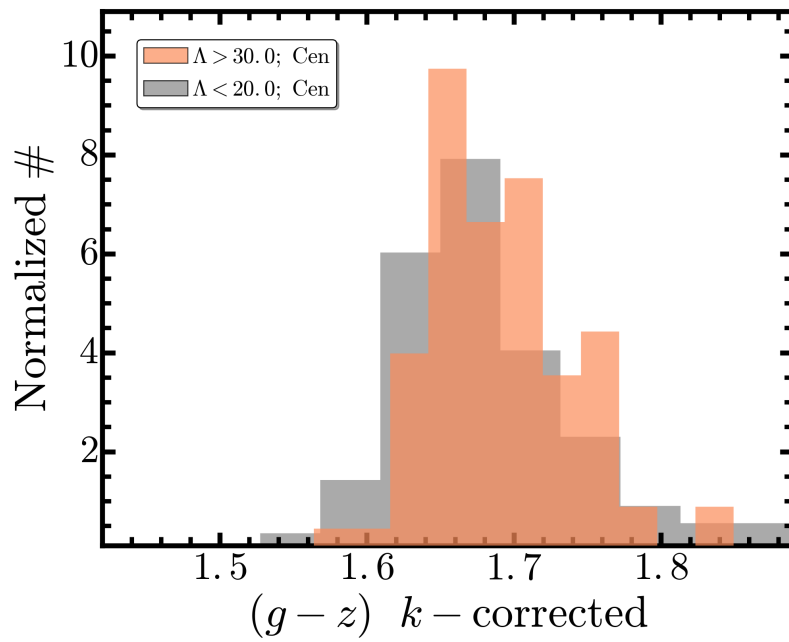


FIG. 3B.— Figure.3b TODO: Caption

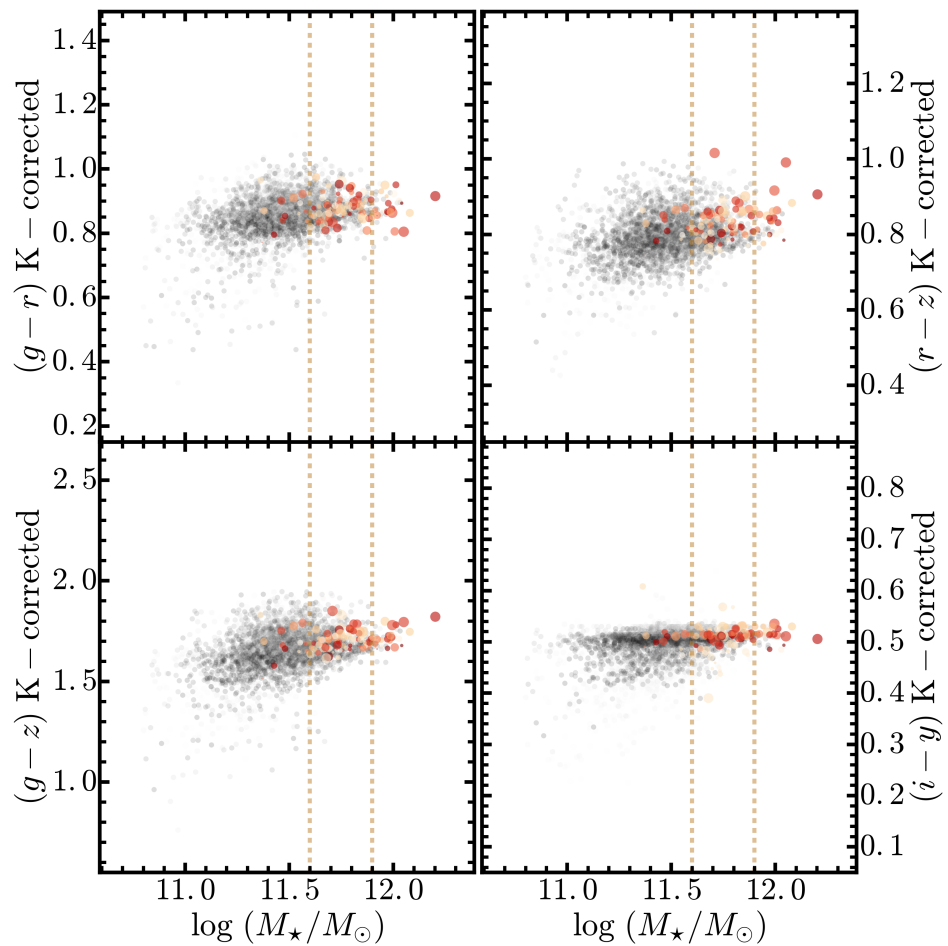


FIG. 3C.— Figure.3c TODO: Caption

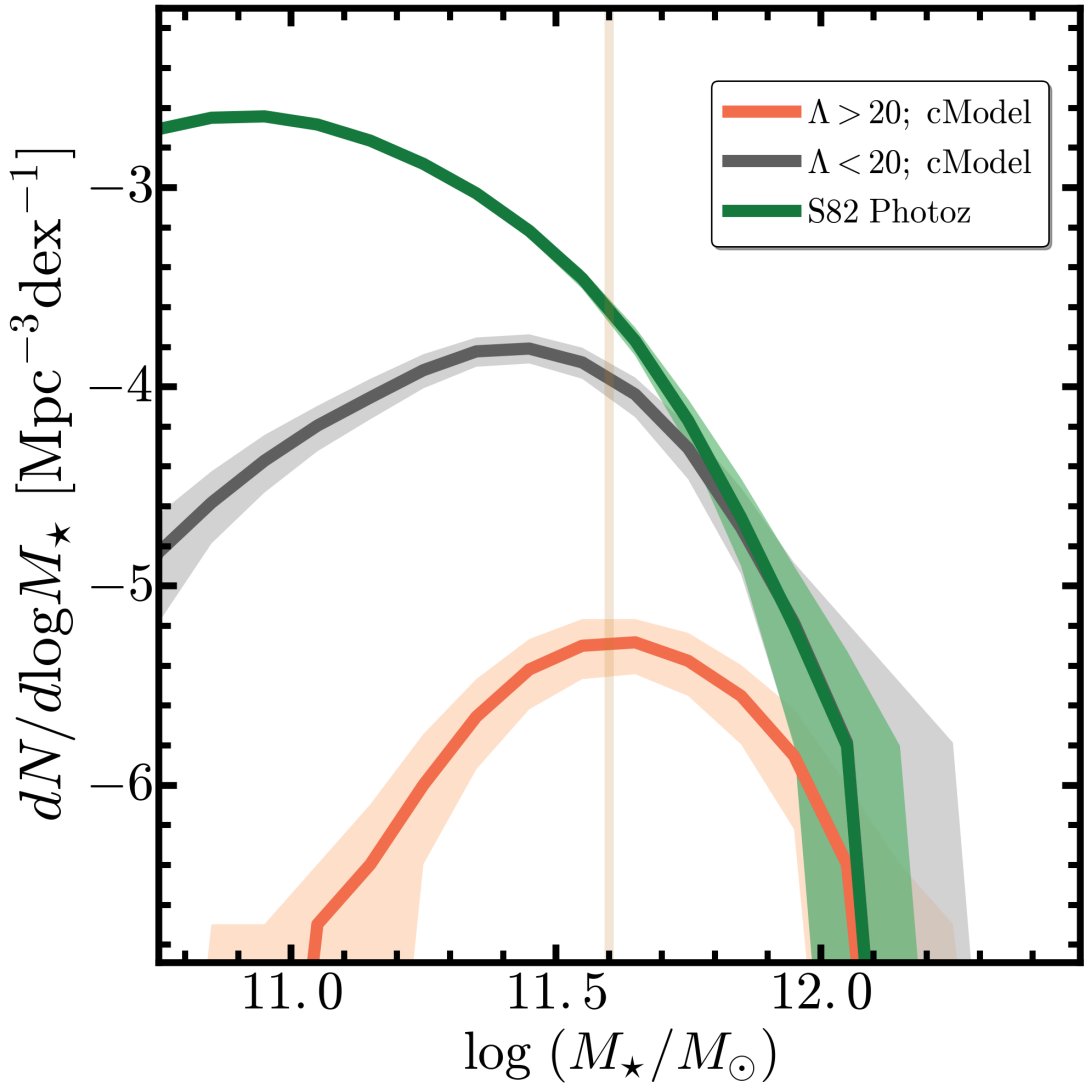


FIG. 4.— Figure.4**TODO: Caption**

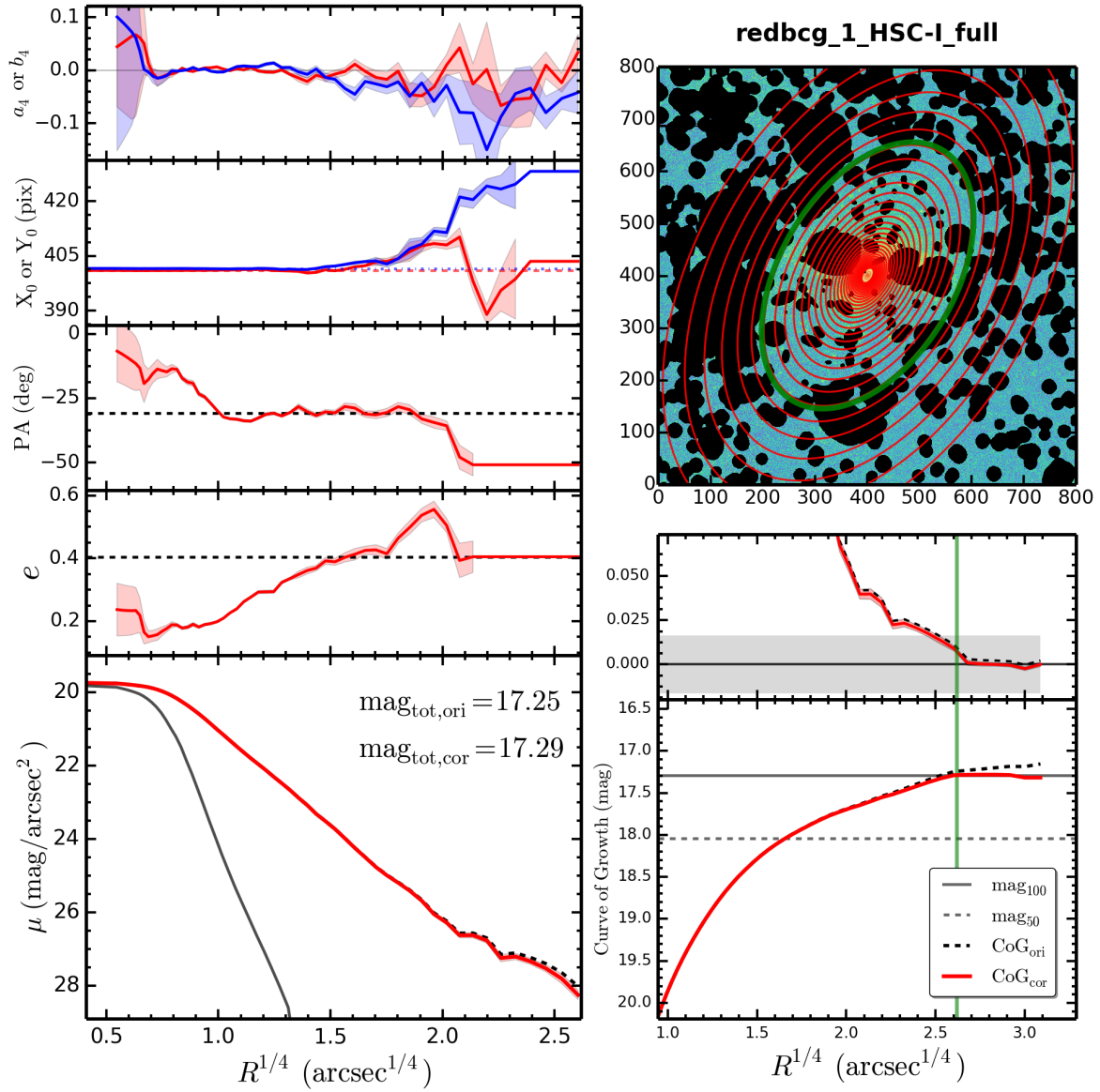


FIG. 5.— Figure 5 TODO: Caption

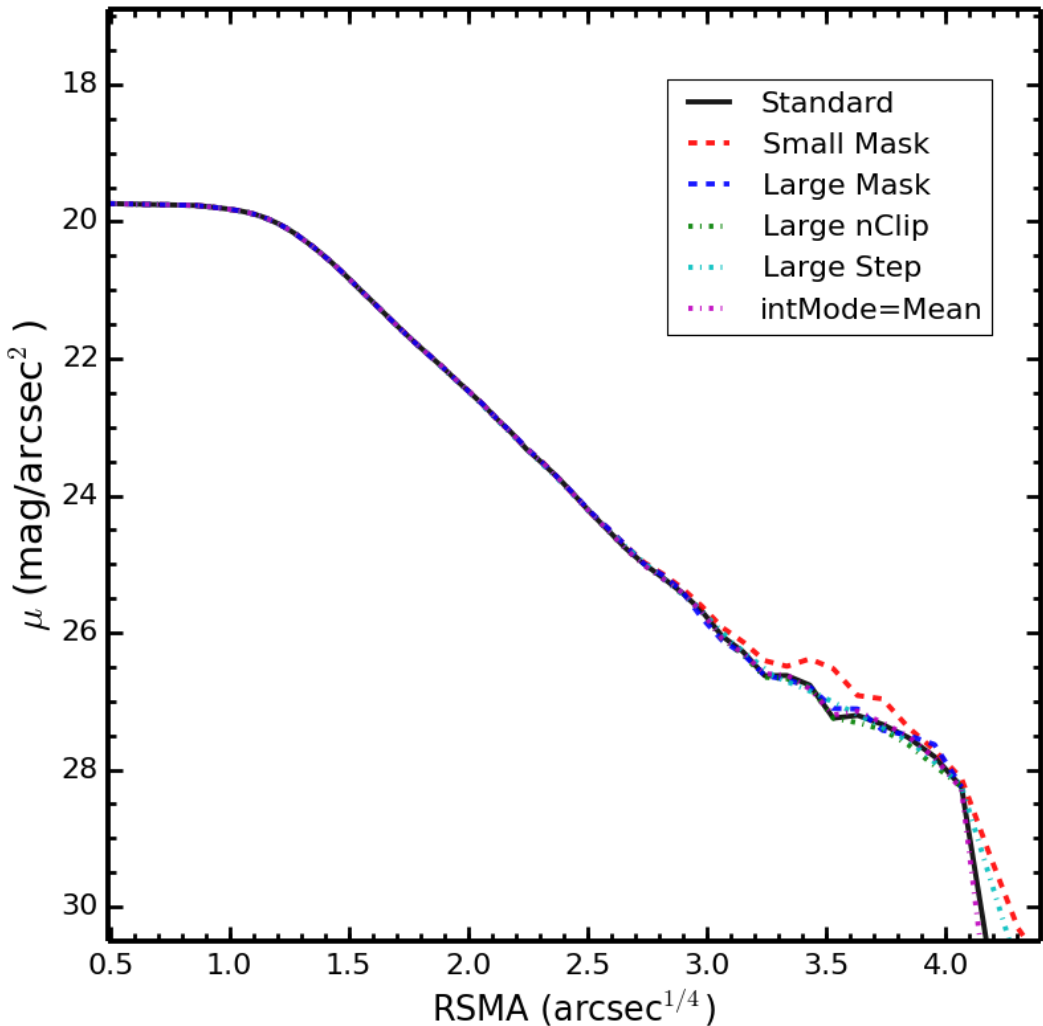


FIG. 6.— Figure.6**TODO: Caption**